Theoretical Chemistry Accounts (2019) 138:111
https://doi.org/10.1007/s00214-019-2495-1

REGULAR ARTICLE

Thermal rate coefficients and kinetic isotope effects of the reaction $HO + H_2O \rightarrow H_2O + OH$

Yongfa Zhu[1,2] · Yunpeng Lu[3] · Hongwei Song[1]

Received: 25 July 2019 / Accepted: 12 August 2019 / Published online: 30 August 2019

Abstract
Hydrogen-transfer reactions take place in a wide range of chemically active environments. In this work, thermal rate coefficients of the prototypical hydrogen-transfer reaction $HO + H_2O \rightarrow H_2O + OH$ and its various isotopologues are computed using both tunneling-corrected transition state and quasi-classical trajectory methods on a recently developed global potential energy surface. On the one hand, the calculated rate coefficients and kinetic isotope effects agree well with available experimental results, indicating the high fidelity of the potential energy surface. On the other hand, the observed normal primary and inverse secondary kinetic isotope effects appear to be prevalent in hydrogen abstraction reactions, which are rationalized by the change of classical and adiabatic minimum energy paths. In addition, there exists strong non-Arrhenius behavior at low temperatures due to the significant quantum tunneling effect.

Keywords Hydrogen-transfer reaction · Kinetic isotope effects · Quantum tunneling effect · Transition state theory · Quasi-classical trajectory

1 Introduction

The prototypical hydrogen exchange reaction

$$HO + H_2O \rightarrow H_2O + OH \quad \text{(R1)}$$

has attracted considerable interest due to its importance in a wide range of chemically active environments [1–16]. The reaction is intrinsically interesting because the associated isotope exchange reactions

$$H^{18}O + H_2O \rightarrow H^{18}OH + OH \quad \text{(R2)}$$

$$DO + H_2O \rightarrow DOH + OH \quad \text{(R3)}$$

$$HO + D_2O \rightarrow HOD + OD \quad \text{(R4)}$$

could affect the isotopic composition of the stratospheric water, a knowledge of which is useful to validate several atmospheric models [16].

Due to the symmetry of the reaction, experimental measurement of the rate constant of the reaction R1 is unfeasible. Through substituting the reactant OH with OH^{18} and OD and H_2O with D_2O, the rate constants were measured by Dubey et al. [16] to be $(2.2 \pm 1.0) \times 10^{-16}$, $(3 \pm 1.0) \times 10^{-16}$ and 5×10^{-17} cm^3 $molecule^{-1}$ s^{-1} at 300 K for the reactions R2, R3 and R4, respectively. The significantly lower pre-exponential factor of $A = (2.3 \pm 1.0) \times 10^{-13}$ cm^3 $molecule^{-1}$ s^{-1} for the reaction R2 in the temperature range from 300 to 420 K than typical values was attributed to the formation of a hydrogen-bonded pre-reaction complex, leading to an entropic constraint. McCabe et al. [17] reported the rate coefficients for the vibrational relaxation of OH ($\nu = 1$) and OD ($\nu = 1$) by H_2O and D_2O at temperatures from 251 to 390 K. They proposed that the transient formation of hydrogen-bonded complexes in the relaxation process can undergo intramolecular vibrational redistribution at a rate competitive with their re-dissociation.

Theoretically, the kinetics of the reaction has been studied using different theories, including canonical variational

✉ Yunpeng Lu
yplu@ntu.edu.sg

✉ Hongwei Song
hwsong@wipm.ac.cn

[1] State Key Laboratory of Magnetic Resonance and Atomic and Molecular Physics, Wuhan Institute of Physics and Mathematics, Chinese Academy of Sciences, Wuhan 430071, China

[2] University of Chinese Academy of Sciences, Beijing 100049, China

[3] Division of Chemistry and Biological Chemistry, School of Physical and Mathematical Sciences, Nanyang Technological University, Singapore 637371, Singapore

transition state theory (CVT) or transition state theory (TST) with/without tunneling correction [14, 18], semi-classical variational transition state theory (SVTST) [15] and quantum reaction path Hamiltonian method [19]. These studies demonstrated that the tunneling effect is very important especially at low temperatures. Recently, Gao et al. [20] investigated the stationary points along the reaction path of the $HO + H_2O$ reaction using the "gold standard" CCSD(T) method with the correlation-consistent basis sets up to the augmented correlation-consistent polarized quintuple zeta basis set (aug-cc-pV5Z). Bai et al. [21] reported a full-dimensional permutation invariant polynomial neural network [22–25] potential energy surface (PIP-NN PES) for the title reaction at the level of CCSD(T)-F12a/aug-cc-pVTZ with a total root-mean-squared error (RMSE) of 0.12 kcal mol^{-1}. A new global, full-dimensional ground-state PES was then constructed by our group using the fundamental invariant neural network (FI-NN) method [26–28], which has similar RMSE to the PIP-NN PES. The mode-specific dynamics and energy flow in the reaction were studied in the FI-NN PES [29].

In this work, thermal rate coefficients for the title reaction (R1) and its various isotopologues (R2, R3 and R4) will be calculated using the canonical variational transition state theory with multidimensional tunneling effects (CVT/MT) [30, 31], as well as the standard quasi-classical trajectory (QCT) method on the FI-NN PES, aiming at unveiling the kinetic isotope effects. This paper is organized as follows. Section 2 details the theoretical methods, followed by the results and discussion in Sect. 3. Finally, conclusions are given in Sect. 4.

2 Theory

2.1 Quasi-classical trajectory method

Standard QCT calculations are carried out using the software VENUS [32]. The thermal rate coefficients at high temperatures from 500 to 2000 K are calculated by

$$k^{\mathrm{QCT}}(T) = \frac{1}{Q_e}\left(\frac{8k_BT}{\pi\mu}\right)^{1/2}\pi b_{\max}^2\frac{N_r}{N_{tot}} \quad (1)$$

where μ is the reduced mass between the reactants OH and H_2O and k_B is the Boltzmann constant. The electronic partition function Q_e is obtained by $\left(2 + 2e^{-140/k_BT}\right)/2$, in which the spin–orbit splitting of OH is taken as 140 cm^{-1} [33]. N_r and N_{tot} are the numbers of reactive and total trajectories at a specified temperature T. The initial ro-vibrational energies of the two reactants and the collision energy are sampled according to the Boltzmann distribution. At each temperature, the impact parameter b is sampled according to $b = b_{\max}R^{1/2}$, where R is a random number in between 0 and 1. The maximum impact parameter $b_{\max}$ is determined using small batches of trajectories. The relative statistical error is given by $\Delta = \sqrt{\left(N_{tot} - N_r\right)/N_{tot}N_r}$. All the trajectories are involved in the statistics since applying zero-point energy (ZPE) constraints sometime can lead to unphysical results [34].

Batches of trajectories (800,000–1,500,000) are run at each temperature, guaranteeing the statistical errors all below 5%. The trajectories are launched from a reactant separation of 9.0 Å and ended when products or reactants reach a separation of 10.0 Å for reactive or non-reactive trajectories. The time step is taken as 0.05 fs, which conserves the total energy better than 10^{-3} kcal mol^{-1} during the propagation. It should be pointed out that QCT calculations become prohibitive at low temperatures due to the requirement of an extremely large number of trajectories.

2.2 Transition state theory

The thermal rate coefficients are computed with POLYRATE 9.7 [35] in the temperature range of 200–2000 K. According to the canonical variational transition state theory, the CVT/MT rate coefficients are defined as

$$k^{\mathrm{CVT/MT}}(T) = \kappa^{\mathrm{tun}}(T)k^{\mathrm{CVT}}(T), \quad (2)$$

where $\kappa^{\mathrm{tun}}(T)$ denotes the transmission coefficient and $k^{\mathrm{CVT}}(T)$ represents the CVT rate coefficient. Given the importance of multidimensional tunneling correction, tunneling effects are included using the microcanonical optimized multidimensional tunneling (μOMT) approach, in which the larger of the small-curvature (SCT) and large-curvature (LCT) tunneling probabilities is adopted as the best estimate [31, 36]. The vibrational modes orthogonal to the reaction coordinates are treated quantum mechanically within the harmonic approximation using redundant internal coordinates [37–39], except for the torsional mode of the HO group with respect to the OH group in HO–H–HO (the frequency is 351 cm^{-1} on the FI-NN PES) [29]. As has been reported in $OH + CH_4$ reaction [40], this particular type of torsion is a nearly free rotor with an extremely low harmonic frequency while is the most troublesome for CVT calculations. Therefore, the partition function for this torsional mode is treated as a free rotor [40–45]. The rotational partition functions are calculated classically. It needs to be emphasized that the treatment of the torsional problem and the choice of the coordinate system have a significant effect on the kinetics [40].

The minimum energy paths (MEPs) of the $HO + H_2O$ reaction and its isotopologues, initiating from the saddle point geometry and going downhill to the pre- and

Table 1 Energies (in kcal mol^{-1}) of the stationary points and imaginary frequencies of the transition state for the reaction HO + H_2O → H_2O + OH and its isotopologues on the FI-NN PES

Species	Reactant	CP1	CP2	TS2	CP2′	CP1′	Product	TS2
V_C	0.00	−5.88	−3.64	9.09	−3.64	−5.88	0.00	
V_{R1}	0.00	−3.91	−2.30	8.67	−2.30	−3.91	0.00	2007i
V_{R2}	0.00	−3.91	−2.30	8.64	−2.33	−3.94	−0.03	2005i
V_{R3}	0.00	−4.23	−2.38	8.26	−2.72	−4.33	−0.35	2006i
V_{R4}	0.00	−4.04	−2.52	9.44	−2.15	−3.90	0.40	1443i

V_C is the classical potential energy; V_{R1}, V_{R2}, V_{R3} and V_{R4} are the ZPE-corrected energies

post-reaction wells in mass-weighted Cartesian coordinates with a step size of 5.0×10^{-5} amu$^{1/2}$ Å, are analyzed on the FI-NN PES. The reaction coordinate (s) is defined as the signed distance from the saddle point ($s=0$), with $s>0$ referring to the product side and $s<0$ to the reactant side. The Hessian matrix is calculated every 9 steps. Meanwhile, the redundant curvilinear projection formulism is utilized to perform a generalized normal-mode analysis along the reaction coordinate. The ground-state adiabatic potential energy is defined as $V_a^G(s) = V_{MEP}(s) + \varepsilon_{int}(s)$, where $\varepsilon_{int}(s)$ is one-half of the sum of the vibrational frequencies of the generalized normal modes orthogonal to the reaction coordinate s.

3 Results and discussion

3.1 Thermal rate coefficients

The classical and ZPE-corrected energies of the stationary points of the HO + H_2O reaction and its various isotopologues on the FI-NN PES are listed in Table 1, together with the imaginary frequencies of the transition state. Compared with the reaction R1 (HO + H_2O), the adiabatic barrier height for the reaction R3 (DO + H_2O) reduces from 8.67 to 8.26 kcal mol^{-1}, while it raises up to 9.44 kcal mol^{-1} for the reaction R4 (HO + D_2O). The imaginary frequency of the transition state for the reaction R4 is 1443 cm^{-1}, in sharp contrast to the value of about 2000 cm^{-1} for R1, R2 and R3, indicating that the reaction barrier is significantly widened by the deuterium substitution of H in the reactant H_2O. The associated MEPs and vibrational adiabatic ground-state energies are displayed in Fig. 1. Clearly, the profile of the MEP for R4 is visibly wider than the others.

The tunneling effect plays an important role in many hydrogen-transfer reactions [46–55]. Figure 2 depicts the rate coefficients of the HO + H_2O → H_2O + OH with/without tunneling corrections. The CVT/SCT, CVT/COMT and CVT/μOMT methods all give very close rate coefficients, which are significantly larger than the TST and CVT values without tunneling corrections at low temperatures. The CVT/ZCT (ZCT denotes the zero-curvature tunneling) and CVT/LCG4 rate coefficients are in between them. All the methods are utilized to calculate the rate coefficients of the

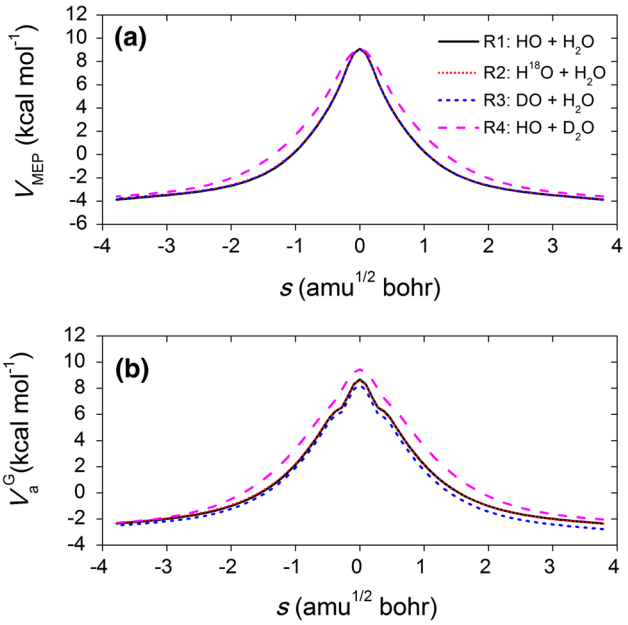

Fig. 1 **a** Minimum energy paths, V_{MEP} and **b** vibrationally adiabatic ground-state energies, V_a^G, of the reaction HO + H_2O → H_2O + OH and its isotopologues as a function of reaction coordinate s

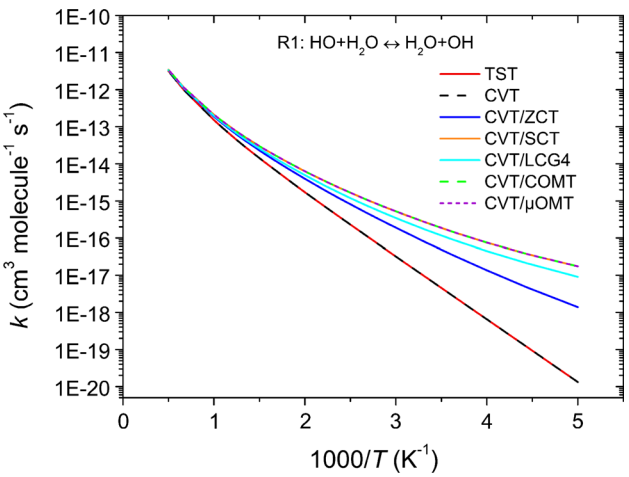

Fig. 2 Calculated thermal rate coefficients for the reaction HO + H_2O → H_2O + OH with different tunneling correction methods

other three isotopic substitution reactions (R2, R3 and R4) and the obtained rate coefficients are compared with experimental values [16]. It is found that the CVT/μOMT method (CVT/SCT and CVT/COMT as well) provides the best estimations. Therefore, the CVT/μOMT results are presented and discussed hereafter. The CVT/μOMT transmission coefficients of the four reactions are plotted in Fig. 3. The large transmission coefficients at low temperatures confirm the importance of the tunneling effect in those reactions. The significant tunneling effect in the reaction is possibly caused by the existence of the two complexes CP1 and CP2 along the MEP. The adiabatic energy profiles for the bimolecular

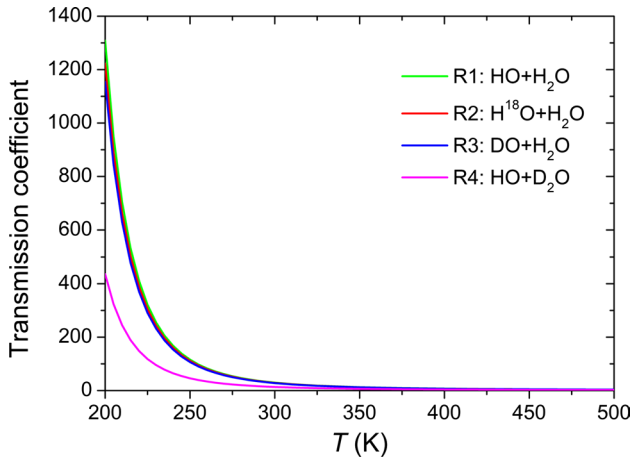

Fig. 3 CVT/μOMT transmission coefficients for the reactions $HO + H_2O \rightarrow H_2O + OH$ and its isotopologues

hydrogen (deuterium) transfer processes without passing through the complexes would be wider than those along the MEP [14, 18]. At low temperatures, the reactions prefer to occur along the MEP and thus the tunneling effect becomes more significant.

Figure 4 shows the calculated thermal rate coefficients for the four reactions R1, R2, R3 and R4 in the temperature range of 200−2000 K. The corresponding values are listed in Table 2. It can be seen that, on the one hand, the CVT/μOMT rate coefficients for the four reactions agree well with the QCT results at high temperatures. The agreement becomes a little worse as the temperature decreases, resulting from the increasing importance of the quantum tunneling effect. Because the tunneling effect is absent in QCT calculations while it is approximately included in the CVT/μOMT treatment. On the other hand, the theoretical rate coefficients exhibit a tunneling facilitated non-Arrhenius behavior at low temperatures. The experimental rate coefficients measured by Dubey et al. [16] at $T = 300$ K are also plotted in the figure, which are well-reproduced by the CVT/μOMT calculations.

3.2 Kinetic isotope effects

Kinetic isotope effects (KIEs) are a valuable tool for the analysis of chemical reaction mechanisms [56]. KIEs are defined as the ratios of k_{R1}/k_{Ri} ($i = 2$–4), in which k_{R1} is the rate constant for the unsubstituted reaction R1 and k_{Ri} stands for the rate constant of the isotopically substituted reactions R2–R4. Since it is impracticable to measure the thermal rate coefficients of

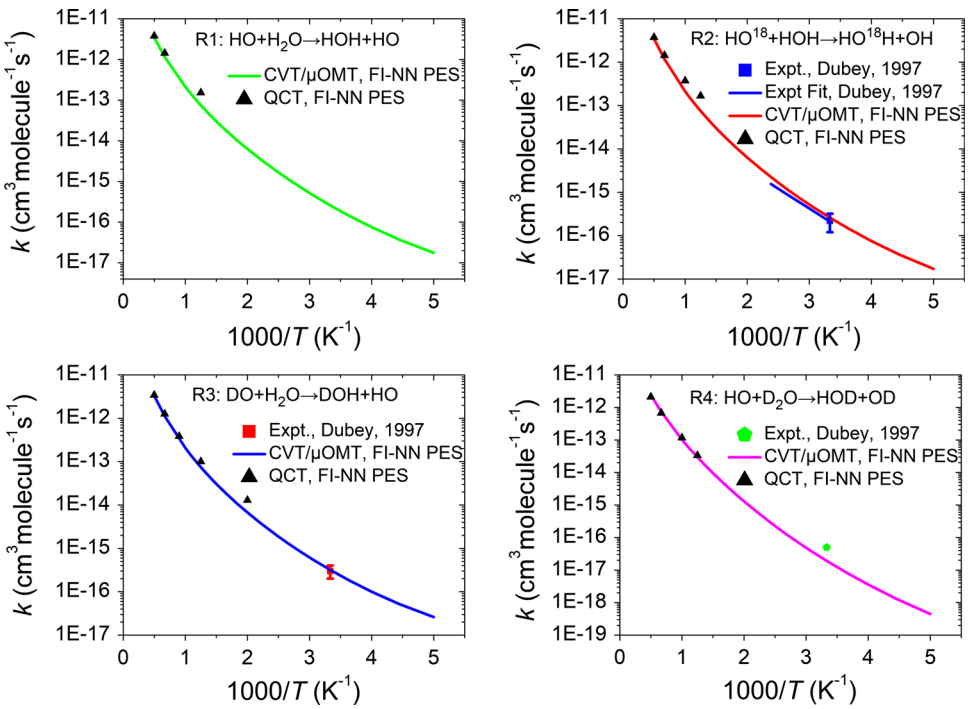

Fig. 4 Theoretical thermal rate coefficients for the reaction $HO + H_2O \rightarrow H_2O + OH$ and its isotopologues in comparison with available experimental values at $T = 300$ K

Table 2 Calculated CVT/μOMT rate constants (in cm^3 $molecule^{-1}$ s^{-1}) (power of 10 in parentheses)

T (K)	R1	R2	R3	R4
200	1.75 (−17)	1.72 (−17)	2.62 (−17)	4.45 (−19)
225	3.73 (−17)	3.69 (−17)	5.22 (−17)	1.34 (−18)
250	7.56 (−17)	7.51 (−17)	1.00 (−16)	3.58 (−18)
275	1.44 (−16)	1.44 (−16)	1.84 (−16)	8.64 (−18)
300	2.59 (−16)	2.59 (−16)	3.19 (−16)	1.91 (−17)
325	4.42 (−16)	4.41 (−16)	5.27 (−16)	3.89 (−17)
350	7.16 (−16)	7.17 (−16)	8.34 (−16)	7.42 (−17)
375	1.11 (−15)	1.11 (−15)	1.27 (−15)	1.33 (−16)
400	1.67 (−15)	1.67 (−15)	1.87 (−15)	2.28 (−16)
420	2.25 (−15)	2.25 (−15)	2.49 (−15)	3.38 (−16)
450	3.41 (−15)	3.42 (−15)	3.71 (−15)	5.84 (−16)
500	6.30 (−15)	6.32 (−15)	6.71 (−15)	1.30 (−15)
550	1.08 (−14)	1.08 (−14)	1.13 (−14)	2.60 (−15)
600	1.73 (−14)	1.73 (−14)	1.79 (−14)	4.75 (−15)
650	2.64 (−14)	2.64 (−14)	2.69 (−14)	8.09 (−15)
700	3.86 (−14)	3.87 (−14)	3.91 (−14)	1.30 (−14)
750	5.45 (−14)	5.46 (−14)	5.47 (−14)	2.00 (−14)
800	7.48 (−14)	7.49 (−14)	7.46 (−14)	2.94 (−14)
850	9.99 (−14)	1.00 (−13)	9.91 (−14)	4.19 (−14)
900	1.31 (−13)	1.31 (−13)	1.29 (−13)	5.78 (−14)
950	1.68 (−13)	1.68 (−13)	1.65 (−13)	7.79 (−14)
1000	2.11 (−13)	2.12 (−13)	2.07 (−13)	1.03 (−13)
1250	5.55 (−13)	5.56 (−13)	5.38 (−13)	3.16 (−13)
1500	1.16 (−12)	1.17 (−12)	1.12 (−12)	7.30 (−13)
1750	2.11 (−12)	2.11 (−12)	2.02 (−12)	1.41 (−12)
2000	3.45 (−12)	3.45 (−12)	3.29 (−12)	2.41 (−12)

the symmetric reaction R1, the ratios of k_{R3}/k_{R2} and k_{R4}/k_{R3} are calculated to compare with the experimental values measured by Masgrau et al. [14]. As shown in the upper panel in Fig. 5, the theoretical ratio of k_{R3}/k_{R2} is 1.23 at $T = 300$ K, close to the experimental value of 1.32. Obviously, substituting $H^{18}O$ by DO enhances the reactivity because the reduction in ZPE caused by the isotopic substitution is larger at the tight transition state than for the reactants. Three additional modes (OD stretch, DOH bend, OD torsion) are altered at the DO–H–OH transition state, while only one mode is affected in the reactants (OD stretch). As the temperature rises to 1000 K, the ratio of k_{R3}/k_{R2} becomes nearly unchanged with a value of about 1, which means that the isotope substitution effect ($H^{18}O$ by DO) is negligible at high temperatures.

The ratio of k_{R4}/k_{R3} is plotted in the lower panel in Fig. 5. The theoretical value is 0.06 at $T = 300$ K, well-located below the experimental upper limit of 0.17. Substituting H_2O by D_2O and OD by OH decreases the reactivity substantially at low temperatures. As the temperature goes up, the isotope substitution effect becomes weak as well. Although the ZPEs of the DO–H–OH and HO–D–OD transition states

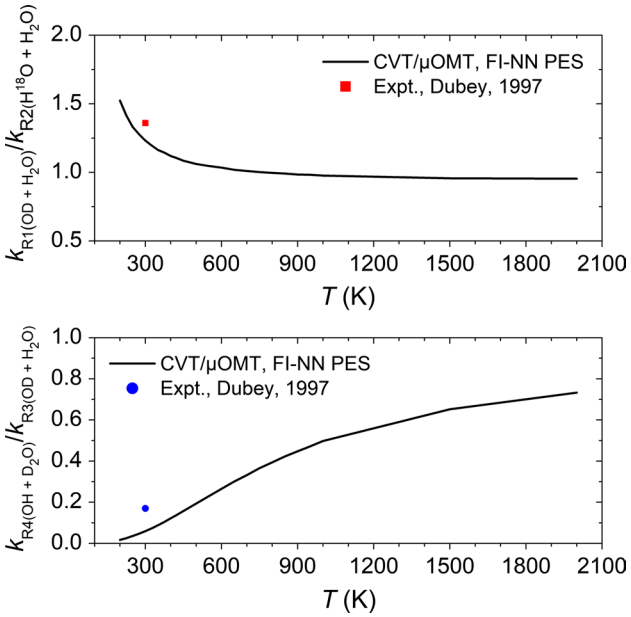

Fig. 5 Comparison of theoretical and experimental ratios of k_{R3}/k_{R2} and k_{R4}/k_{R3}

are similar, the total ZPE of the reactants OH and D_2O is lower than that of OD and H_2O.

The theoretical KIEs according to the standard definition are presented in Fig. 6. The reaction R4 ($HO + D_2O$) shows a normal primary KIE (> 1) over the temperature range studied. Because the transferring deuterium has a lower vibrational frequency in between OH and DO, resulting in smaller tunneling probability through the reaction barrier than the hydrogen in R1 ($HO + H_2O$). On the other hand, the adiabatic barrier for R4, as shown in the lower panel in Fig. 1 in mass-scaled coordinates, is not only higher but also thicker than that for R1.

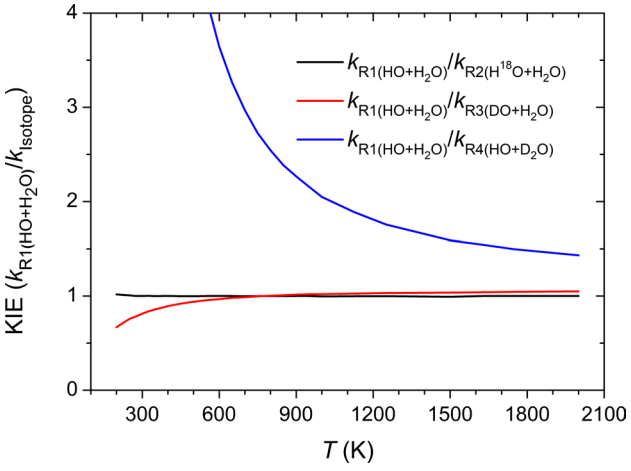

Fig. 6 Calculated kinetic isotope effects (KIEs) as a function of the temperature over the range of 200 – 2000 K

The reaction R3 ($DO + H_2O$) shows an inverse secondary KIE at low temperatures as $k_{R1}/k_{R3} < 1$. As the temperatures increases, the ratio of k_{R1}/k_{R3} becomes nearly a constant with a value slightly larger than 1. It can also be rationalized by the difference of V_a^G plotted in Fig. 1. The deuterated atom in the reactant OD does not affect V_{MEP} very much, but the V_a^G for $DO + H_2O$ is somewhat thinner than that for $HO + H_2O$ reaction in transition state region, which governs the kinetics. In addition, substituting HO by $H^{18}O$ has a negligible KIE over the temperature range studied.

The primary and second KIEs observed in the reaction $HO + H_2O \rightarrow H_2O + OH$ appear to be prevalent in polyatomic hydrogen abstraction reactions. The normal primary and inverse secondary KIEs have also been observed in other reactions at temperatures above 200 K, such as $CH_3 + HBr \rightarrow CH_4 + Br$ [57], $OH + CH_4 \rightarrow H_2O + CH_3$ [58] and $H + C_2H_6 \rightarrow H_2 + C_2H_5$ [59]. The quantum tunneling effect is expected to play an important role in these reactions, especially at low temperatures.

4 Conclusions

In this work, we investigate the kinetics of gas-phase hydrogen abstraction reaction, $HO + H_2O \rightarrow H_2O + OH$ reaction and its various isotopologues using both the transition state theory with multidimensional tunneling (CVT/μOMT) and the QCT method on an accurate global PES. The good agreements between the experimental and theoretical KIEs provide strong evidence on the accuracy of the FI-NN PES. It is found that the tunneling effect plays a significant role at low and moderate temperatures. The existence of the complexes actuates a faster fall of the adiabatic potential energy moving away from the transition state, reduces the width of the classical forbidden region, and thus results in large tunneling effects.

Acknowledgements This work was supported by the National Natural Science Foundation of China under Grant No. 21603266

References

1. Atkinson R (1986) Chem Rev 86:69
2. Nanayakkara AA, Balintkurti GG, Williams IH (1992) J Phys Chem 96:3662
3. Arnold DW, Xu C, Neumark DM (1995) J Chem Phys 102:6088
4. Langford VS, McKinley AJ, Quickenden TI (2000) J Am Chem Soc 122:12859
5. Hamad S, Lago S, Mejias JA (2002) J Phys Chem A 106:9104
6. Smith IWM, Ravishankara AR (2002) J Phys Chem A 106:4798
7. Cabral do Couto P, Guedes RC, Costa Cabral BJ, Martinho Simões JA (2003) J Chem Phys 119:7344
8. Marshall MD, Lester MI (2005) J Phys Chem B 109:8400
9. Wilson B (2005) Chem Eng News 83:39
10. Allodi MA, Dunn ME, Livada J, Kirschner KN, Shields GC (2006) J Phys Chem A 110:13283
11. McCabe DC, Rajakumar B, Marshall P, Smith IWM, Ravishankara AR (2006) Phys Chem Chem Phys 8:4563
12. Cooper WJ, Cramer CJ, Martin NH, Mezyk SP, O'Shea KE, von Sonntag C (2009) Chem Rev 109:1302
13. Codorniu-Hernandez E, Kusalik PG (2012) J Am Chem Soc 134:532
14. Masgrau L, Gonzalez-Lafont A, Lluch JM (1999) J Phys Chem A 103:1044
15. Hand MR, Rodriquez CF, Williams IH, Balint-Kurti GG (1998) J Phys Chem A 102:5958
16. Dubey MK, Mohrschladt R, Donahue NM, Anderson JG (1997) J Phys Chem A 101:1494
17. McCabe DC, Rajakumar B, Marshall P, Smith IW, Ravishankara AR (2006) Phys Chem Chem Phys 8:4563
18. Uchimaru T, Chandra AK, Tsuzuki S, Sugie M, Sekiya A (2003) J Comput Chem 24:1538
19. Gonzalez J, Caballero M, Aguilar-Mogas A, Torrent-Sucarrat M, Crehuet R, Solé A, Giménez X, Olivella S, Bofill JM, Anglada JM (2010) Theor Chem Acc 128:579
20. Gao A, Li G, Peng B, Xie Y, Schaefer HF (2016) J Phys Chem A 120:10223
21. Bai M, Lu D, Li J (2017) Phys Chem Chem Phys 19:17718
22. Xie Z, Bowman JM (2010) J Chem Theory Comput 6:26
23. Jiang B, Guo H (2013) J Chem Phys 139:054112
24. Li J, Jiang B, Guo H (2013) J Chem Phys 139:204103
25. Jiang B, Li J, Guo H (2016) Int Rev Phys Chem 35:479
26. Shao K, Chen J, Zhao Z, Zhang DH (2016) J Chem Phys 145:071101
27. Ping L, Zhu Y, Li A, Song H, Li Y, Yang M (2018) Phys Chem Chem Phys 20:26315
28. Tian L, Zhu Y, Song H, Yang M (2019) Phys Chem Chem Phys 21:11385
29. Zhu Y, Ping L, Bai M, Liu Y, Song H, Li J, Yang M (2018) Phys Chem Chem Phys 20:12543
30. Garrett BC, Truhlar DG (1979) J Am Chem Soc 101:4534
31. Truhlar DG, Issacson, AD, Garrett BC (1985) Generalized transition state theory. In: Baer M (ed) Theory of chemical reaction dynamics. CRC Press, Boca Raton, FL, p 65
32. Hase WL, Duchovic RJ, Hu X, Komornicki A, Lim KF, Lu D-H, Peslherbe GH, Swamy KN, Linde SRV, Varandas A, Wang H, Wolf RJ (1996) Quantum Chem Program Exch Bull 16:671
33. Herzberg G (1940) J Phys Chem 44:954
34. Guo Y, Thompson DL, Sewell TD (1996) J Chem Phys 104:576
35. Zheng J, Bao JL, Meana-Pañeda R, Zhang S, Lynch BJ, Corchado JC, Chuang Y-Y, Fast PL, Hu W-P, Liu Y-P, Lynch GC, Nguyen KA, Jackels CF, Ramos AF, Ellingson BA, Melissas VS, Villà J, Rossi I, Coitiño EL, Pu J, Albu TV (2007) POLYRATE, version 9.7, vol Department of Chemistry and Supercomputing Institute, University of Minnesota, Minneapolis, Minnesota 55455
36. Liu YP, Lu DH, Gonzalezlafont A, Truhlar DG, Garrett BC (1993) J Am Chem Soc 115:7806
37. Jackels CF, Gu Z, Truhlar DG (1995) J Chem Phys 102:3188
38. Natanson GA, Garrett BC, Truong TN, Joseph T, Truhlar DG (1991) J Chem Phys 94:7875
39. Chuang Y-Y, Truhlar DG (1997) J Phys Chem A 101:3808
40. Ellingson BA, Pu J, Lin H, Zhao Y, Truhlar DG (2007) J Phys Chem A 111:11706
41. Truhlar DG (1991) J Comput Chem 12:266
42. Chuang YY, Truhlar DG (2000) J Chem Phys 112:1221
43. Chuang Y-Y, Truhlar DG (2004) J Chem Phys 121:7036
44. Chuang Y-Y, Truhlar DG (2006) J Chem Phys 124:179903
45. Ellingson BA, Lynch VA, Mielke SL, Truhlar DG (2006) J Chem Phys 125:084305
46. Zhang DH, Light JC (1996) J Chem Phys 104:6184

47. Wu T, Werner HJ, Manthe U (2004) Science 306:2227
48. Li Y, Suleimanov YV, Yang M, Green WH, Guo H (2013) J Phys Chem Lett 4:48
49. Habershon S, Manolopoulos DE, Markland TE, Miller TF 3rd (2013) Annu Rev Phys Chem 64:387
50. Czako G, Bowman JM (2014) J Phys Chem A 118:2839
51. Li J, Jiang B, Song H, Ma J, Zhao B, Dawes R, Guo H (2015) J Phys Chem A 119:4667
52. Song H, Lu Y, Li J, Yang M, Guo H (2016) J Chem Phys 144:164303
53. Fu B, Shan X, Zhang DH, Clary DC (2017) Chem Soc Rev 46:7625
54. Qi J, Lu D, Song H, Li J, Yang M (2017) J Chem Phys 146:124303
55. Kumar SS, Grussie F, Suleimanov YV, Guo H, Kreckel H (2018) Sci Adv 4:eaar3417
56. Gonzalez-Lafont A, Lluch JM (2016) Comput Mol Sci 6:584
57. Espinosa-García J (2002) J Chem Phys 117:276
58. Li J, Guo H (2018) J Phys Chem A 122:2645
59. Espinosa-Garcia J, Corchado JC (2019) Phys Chem Chem Phys 21:13356